metrology

MDPI

Article

Research on Acoustic Properties of Artificial Inhomogeneities in Calibration Samples for Ultrasonic Testing of Polyethylene Pipe Welds

Aleksandr Shikhov [1], Kirill Gogolinskii [2], Darya Kopytina [1,*], Anna Vinogradova [1] and Aleksei Zubarev [3]

[1] Department of Metrology, Instrumentation and Quality Management, Empress Catherine II Saint Petersburg Mining University, 199106 Saint Petersburg, Russia; shihov-gol@mail.ru (A.S.); vinogradova_aa@pers.spmi.ru (A.V.)
[2] Petersburg Nuclear Physics Institute named by B.P. Konstantinov of National Research Centre «Kurchatov Institute», 188300 Gatchina, Russia; nanoscan@yandex.ru
[3] A3 Engineering, 117105 Moscow, Russia; info@a3-eng.com
* Correspondence: daryakopytina2000@yandex.ru; Tel.: +7-(961)-085-4678

Abstract

This article investigates the acoustic properties of artificial discontinuities in reference specimens for the ultrasonic testing of welded joints in polyethylene pipes. An analysis is conducted on the reflectivity of various materials (air, sand, heat-resistant silicate-based sealant, and aluminum foil) and their correspondence to real defects occurring in weld seams. A theoretical analysis of reflection coefficients is performed, along with laboratory studies using digital radiography and ultrasonic testing. The results demonstrate that heat-resistant silicate sealant is the most suitable material for simulating defects, as its acoustic properties closely match those of real inclusions, and its geometric parameters remain stable during the welding process. The use of such specimens enhances the reliability of ultrasonic testing and reduces the likelihood of errors in defect classification.

Keywords: ultrasonic testing; polyethylene pipes; welded joints; artificial discontinuities; reflection coefficient; reference specimens; heat-resistant sealant; digital radiography; metrological support; defects

check for updates

Academic Editor: Steve Vanlanduit

Received: 30 June 2025
Revised: 9 August 2025
Accepted: 11 August 2025
Published: 20 August 2025

Citation: Shikhov, A.; Gogolinskii, K.; Kopytina, D.; Vinogradova, A.; Zubarev, A. Research on Acoustic Properties of Artificial Inhomogeneities in Calibration Samples for Ultrasonic Testing of Polyethylene Pipe Welds. *Metrology* **2025**, *5*, 51. https://doi.org/10.3390/metrology5030051

Copyright: © 2025 by the authors. Licensee MDPI, Basel, Switzerland. This article is an open access article distributed under the terms and conditions of the Creative Commons Attribution (CC BY) license (https://creativecommons.org/licenses/by/4.0/).

1. Introduction

Polyethylene pipes have become widely used in the construction of gas pipelines due to their advantages, including durability [1–3] and resistance to corrosion [4–6]. Structural strength and pressure resistance are critical parameters for gas pipelines, as accidents on such facilities lead to severe consequences: fires, explosions, environmental disasters, and even loss of life [7–9].

One of the reasons for the failure of polyethylene pipelines is the low reliability of welded joints [10–12]. This is evidenced by a number of reports from Russian [13] (Gazprom Group Social Responsibility Report 2023 URL: https://sustainability.gazpromreport.ru/2023/, accessed on 12 January 2025) and foreign companies [14–16]. During welding operations, the quality of welded joints [17,18] is influenced by a significant number of factors, such as heater temperature, welding time, pressure, and non-compliance with the procedure for preparing the surfaces to be welded [19,20].

In this regard, a critical role in ensuring the failure-free operation of pipelines [21,22] should be assigned to the reliability of methods for inspecting welded joints [23–25].

Currently, the ultrasonic method [26–28] of non-destructive testing of polyethylene pipes has gained widespread adoption [29–31].

The reliability of ultrasonic testing largely depends on its metrological support [32]. The metrological support of non-destructive testing constitutes a system of elements and processes required to obtain information about an object's condition with specified properties (GOST R 56510-2015. (2015). Metrological assurance in non-destructive testing [33]). It should be noted that depending on the specific testing objective, the primary informative parameter of ultrasonic testing methodology may vary, as may the required measurement accuracy for this parameter.

In [34], an analysis of uncertainty sources in the ultrasonic testing method was conducted. The authors note that the main contributors to measurement uncertainty are variations in the acoustic and physical-mechanical properties of the test object, instrumental factors (flaw detector–transducer system and reference standards), and methodological factors (calibration and inspection procedures).

To determine the assigned (normalized) values of the characteristics of a flaw detector–transducer pair, various methodologies can be used. Ref. [35] describes a method for determining the spatial characteristics of an ultrasonic pulse, such as the angle of incidence and the directivity pattern. The proposed method involves visualizing the echo pulse by measuring the three-dimensional coordinates of a spherical tracer particle. To evaluate the transducer's transfer function, a calibration hydrophone recording the time-varying acoustic pressure is most commonly used [36]. Ref. [37] proposes an alternative method for determining the transducer's transfer function. It is based on the relationship between the acoustic flow velocity and the sound intensity on the transducer's surface. To measure the acoustic flow velocity of a liquid, ink is used as a tracer, along with a digital camera.

From the standpoint of inspection reliability, the actual values of metrological characteristics are more critical. These values are determined based on the normalized ones but take into account the physical and mechanical properties of the test object. In ultrasonic testing practice, this procedure is most commonly referred to as establishing the basic inspection parameters. In conventional flaw detection, such parameters include, for example, the angle of incidence, timebase calibration, dead zone, and sensitivity level.

The reliability of classifying a detected discontinuity as a "defect" and the accuracy of assessing its dimensions and spatial position largely depend on the correctly set sensitivity. The quantitative parameter of sensitivity is the sensitivity level, which, depending on its functional purpose, can be reference, rejection, or detection level. In the case of the rejection sensitivity level, the decision on the acceptability of a discontinuity is made based on the echo amplitude [38].

For determining the main inspection parameters of steel and aluminum products, calibration blocks such as SO-2,34, V1, V2 [39], and KUSOT 180 (Kusot 180 [Kycot 180]. (n.d.). Constanta-US. Retrieved 1 August 2025, from https://constanta-us.com/catalog/nabor_kusot_180/kusot_180_nabor_3/ [40]) are used [41,42]. Depending on the application, these blocks may contain reflectors including backwall surfaces, side-drilled holes (SDHs), and notches. The range also includes blocks with segmented reflectors, angular reflectors (nicks), and flat-bottom holes (FBHs) that simulate surface-breaking defects in welded joints (Reference specimen, flat with notch [Nastroechnyy obrazets, ploskiy s zarubkoy]. (n.d.). Constanta-US. Retrieved 1 August 2025, from https://www.constanta-us.com/catalog/nastroechnye_obraztsy_no/nastroechnyy_obrazets_no_ploskiy_s_zarubkoy/ [43]) [38]. It should be noted that the defect simulators in these reference blocks are characterized by an air/metal acoustic boundary.

For the calibration of the basic testing parameters during the inspection of polyethylene pipeline welds, calibration blocks made from polyethylene pipe sections are used, with

acoustic and geometric parameters equivalent to the test object (Figure 1) (GOST R 8.637-2007. (2007). State system for ensuring the uniformity of measurements. Reference materials for metrological support of pipeline non-destructive testing means [44]). In these calibration blocks, defects are simulated using reflectors in the form of flat-bottom holes with an air/polyethylene acoustic boundary, following the same principle as the calibration blocks for the ultrasonic testing of steel welds.

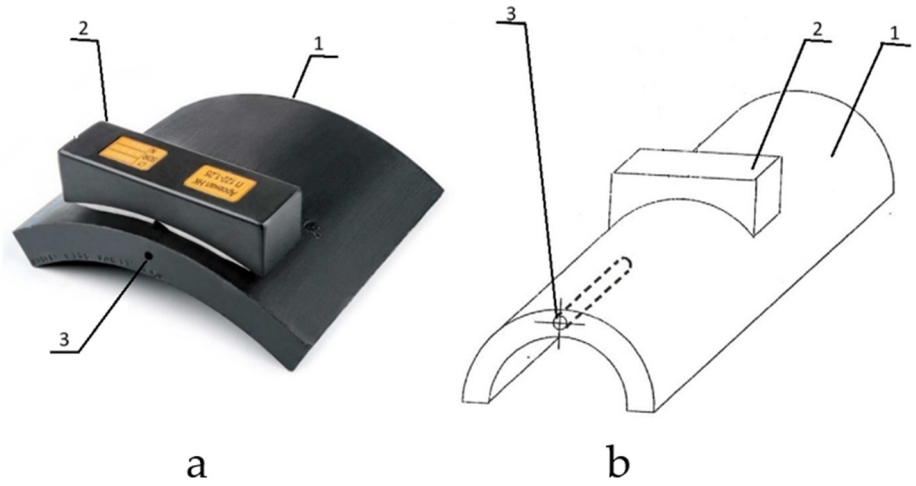


Figure 1. Calibration sample: (**a**) external view; (**b**) schematic. 1—calibration sample; 2—chord-type piezoelectric transducer; 3—artificial reflector.

According to normative documentation (ISO 13588:2012. Non-destructive testing of welds—Ultrasonic testing—Use of automated phased array technology [45]), the calibration blocks for the ultrasonic testing of welded joints shall contain reflectors of established dimensions and shall be fabricated from materials equivalent to those being inspected. These requirements [37] are confirmed by research results in works [46–48], where the authors note that artificial reflectors simulating defects must account for the form, dimensions, orientation, and correlation of acoustic properties with actual defects.

In accordance with the above, the approach to defect simulation in steel calibration blocks is explained by the fact that, due to steel's high acoustic impedance value, the acoustic boundary with discontinuities characteristic of welded joints in steel components is practically acoustically opaque. This means that the majority of the wave energy reflects from the discontinuity (defect). From this perspective, the steel/air boundary is equivalent to the actual defect/steel boundary.

At the same time, welded joints in polyethylene pipes may contain inclusions with density exceeding that of polyethylene, such as sand or soil particles. Since the acoustic properties of air are not equivalent to those of typical discontinuities occurring in polyethylene pipe welds, their reflectivity differs. Consequently, establishing the rejection sensitivity level using calibration blocks with flat-bottom holes during inspection may lead to a situation where the signal from an unacceptable-sized discontinuity falls below the rejection level and the discontinuity is not classified as a defect (Figure 2), resulting in under-rejection (GOST R 50.04.07-2022. Conformity assessment system in the field of atomic energy use. Conformity assessment in the form of testing. Certification testing of non-destructive control systems [49]).

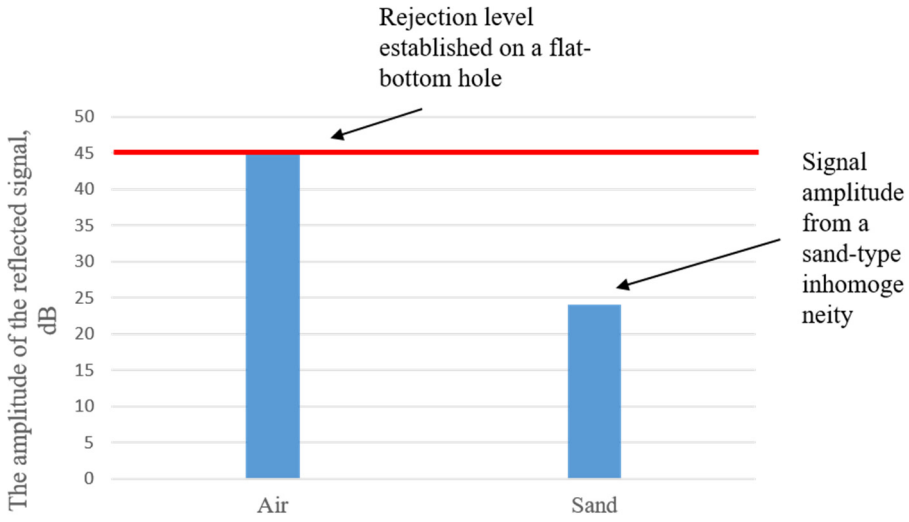


Figure 2. Signal amplitude from a sand inclusion compared to the rejection threshold.

Therefore, it is necessary to develop calibration specimens with reflectors whose properties match those of actual defects occurring in welded joints of polyethylene pipelines. For this purpose, this work has analyzed the acoustic path of reflected signals from inhomogeneities with different properties and evaluated the probability of defect detection using the pulse-echo method.

2. Materials and Methods

2.1. Theoretical Analysis of Reflected Wave Fields

The use of a rejection sensitivity level during inspection involves comparing the amplitudes of reflected signals from the detected inhomogeneity and from the maximum allowable-sized inhomogeneity for the test object. Based on the comparison result, a conclusion is made regarding the classification of the detected inhomogeneity as a defect.

Given that the acoustic properties of the calibration specimen must be equivalent to those of the test object, the task of evaluating signal levels from the inhomogeneity and the reflector is reduced to analyzing the wave field during incidence and reflection at the interface between two media.

Since for normal wave incidence the reflection is always specular (i.e., the difference between the profiles of the incident and reflected waves consists only of a constant multiplier [50], the problem is reduced to analyzing this multiplier, which determines the pressure difference in the acoustic fields of the incident and reflected waves—the reflection coefficient:

$$p_o = R_P p_i; \quad (1)$$

where R_P—reflected-to-incident pressure ratio; p_o, p_i—pressure in the reflected and incident waves, respectively.

The reflection coefficient magnitude is determined by the Fresnel formula:

$$R_p = (\rho_2 c_2 - \rho_1 c_1)/(\rho_2 c_2 + \rho_1 c_1); \quad (2)$$

where ρ—density of the medium; c—speed of sound wave propagation in the medium; subscripts 1 and 2 describe the properties of the medium (test object) and inhomogeneity, respectively.

The Fresnel formulas represent the solution to the system of Equation (5), which describes the boundary conditions (4) for determining the reflection coefficient

magnitude—specifically, the equality of particle velocities and pressure on both sides of the reflector:

$$v = (1/\rho c)p; \tag{3}$$

$$\begin{cases} p_{\text{i}} + p_o = p_{\text{tw}} \\ v_{\text{i}} + v_o = v_{\text{tw}} \end{cases}; \tag{4}$$

$$\begin{cases} 1 + R_p = D_p \\ \frac{1}{\rho c}(1 - R_p) = D_p \end{cases}; \tag{5}$$

where υ—particle velocity; tw—subscript denoting transmitted wave; D_p—pressure transmission coefficient.

Expression (2) was derived for normal wave incidence. However, when inspecting pipe welded joints using the pulse-echo method, oblique incidence must be considered since angled and chord-type transducers are employed. For oblique incidence, the expression for determining the transmission coefficient is derived from boundary conditions (4), supplemented with an equation describing Snell's law. Accordingly, the reflection coefficient is determined by the following expression:

$$R_p = \frac{mcos\theta_1 - ncos\theta_2}{mcos\theta_1 + ncos\theta_2}; \tag{6}$$

where θ_1, θ_2—angles of incidence and refraction, respectively; m = ρ_2/ρ_1; n = c_1/c_2.

Unlike normal incidence, oblique incidence does not always result in specular reflection. For specular reflection to occur, certain conditions must be met, determined by the ratio of wave velocities in the two media. However, since we are considering the conventional pulse-echo method that analyzes the coherent field of a harmonic wave (for which Fresnel formulas are always applicable [29]), these conditions can be neglected.

Analysis of Expression (6) shows that the reflectivity of an inhomogeneity depends both on the parameters of the test object and on the parameters of the inhomogeneity itself. Moreover, under oblique incidence, it is also determined by the transducer parameters, particularly the wave entry angle (angle of incidence). Given that both inspection and the establishment of the rejection sensitivity level must be performed using the same transducer, the influence of the entry angle factor can be disregarded when analyzing the reflectivity of inhomogeneities. Consequently, by assuming specular reflection for oblique wave incidence, the reflectivity analysis can be performed using Expression (2).

It should be noted that the above analysis describes reflection at the boundary of semi-infinite media. However, discontinuities simulating defects have finite dimensions. Consequently, the amplitude of the reflected signal will be determined not only by the characteristics of the acoustic boundary but also by the following:

1. Interference between the incident and multiply reflected waves within the discontinuity volume.

The signal scattered by the discontinuity may be formed through interference of multiple wave components. The resultant interference pattern of the wave field components will depend on the discontinuity's dimensions and orientation, as well as the wave's angle of incidence. Among the reflectors under consideration, only "sand" and "sealant" type discontinuities exhibit volumetric characteristics. The acoustic boundaries of these reflector types are nearly transparent, causing most of the incident wave energy to convert into a refracted wave of the same mode—meaning that the wave essentially transmits through the finite discontinuity volume.

2. Surface roughness of the reflecting boundary. To evaluate the influence of the reflector's surface roughness, the Rayleigh parameter was calculated:

$$P = 2kR_a\cos\alpha \quad (7)$$

where k—wavenumber; R_a—root mean square (RMS) surface roughness height; α—wave entry angle.

The calculation results are presented in Table 1. The surface roughness parameters for the flat-bottom hole were taken from open sources, while those for the foil and sealant were measured using a Hommel-Etamic T1000 Basic profilometer. The roughness of the "sand" type discontinuity was determined based on the average pore size of silty sand. As evident from the data in Table 1, the Rayleigh parameter values for all discontinuity types are significantly below 1, indicating that the surface roughness of the reflectors has negligible influence on the reflected signal amplitude ratios.

Table 1. Rayleigh parameter values for the investigated reflectors.

Reflector Type	Frequency (MHz)	Wave Velocity (m/s)	R_a, mm	Incident Angle (Deg)	Rayleigh Parameter
Flat-bottom hole	1.8	2150	0.025	45	0.26
Sand			0.027		0.29
Sealant			0.018		0.19
Foil			0.0004		0.004

3. Relationship between the ultrasonic beam directivity characteristics and the discontinuity area.

In this case, the amplitude of the reflected signal will be determined by the ratio of the discontinuity area to the area of the incident acoustic field, which is defined by the transducer's far-field beam width. Furthermore, since the far-field beam pattern has a truncated conical shape, the distance from the transducer surface to the discontinuity (reflector) surface will also affect this area ratio. For the defect detection probability analysis in this study, all reflectors were fabricated at the pipe end. After welding, each reflector was positioned at the center of the weld joint, while the transducer was placed flush against the flash edge (weld bead), whose size is determined by the pipe wall thickness. All discontinuity types created in this work represented flat reflectors at the test object/discontinuity interface. Therefore, with other conditions being equal and reflector areas identical, the ratio of reflected signal amplitudes from different discontinuity types will be determined by the reflection coefficient, as expressed in Equation (2).

2.2. Analysis of Reflection Coefficients

Reflection coefficients at polyethylene/air (flat-bottom hole) and polyethylene/sand interfaces are presented in Table 2.

Table 2. Reflection and transmission coefficients at polyethylene interfaces with other media.

No. (Type)	Material	Density (g/cm^3)	Wave Velocity (m/s)	Interface Type	$\lvert R_p \rvert$
1	Air	0.00122	340	Polyethylene/air	0.99
2	Sand	2.00000	1660	Polyethylene/sand	0.25
3	Heat-resistant silicate sealant	2.40000	1531	Polyethylene/sealant	0.29
4	Aluminum foil	2.70000	6250	Polyethylene/foil	0.79
5	Polyethylene	0.92000	2150	-	-

From Table 2, it is evident that the reflection coefficients for Type 1 and 2 interfaces (air and sand) differ significantly. The amplitude of a signal reflected from a sand-filled inhomogeneity will differ from that reflected by an air-filled inhomogeneity of the same size, proportional to the ratio of the reflection coefficients listed in Table 2. Thus, calibration using specimens with air-filled reflectors (flat-bottom holes) during the inspection of butt-welded joints in polyethylene pipelines may increase the probability of Type I and Type II errors.

Accordingly, improving defect detection probability in butt welds can be achieved by selecting a material with acoustic properties similar to real defects in test objects (GOST R 54792-2024. (2024). Defects in welded joints of thermoplastics. Description and evaluation [51]). Furthermore, the stability of this material's properties must be ensured to validate the metrological characteristics of such reflectors.

Aluminum foil and heat-resistant silicate sealant were selected as defect simulators. Key selection criteria included the retention of physical-mechanical properties at welding temperatures (220 °C). Comparative acoustic properties of these materials are shown in Table 2 and Figure 3.

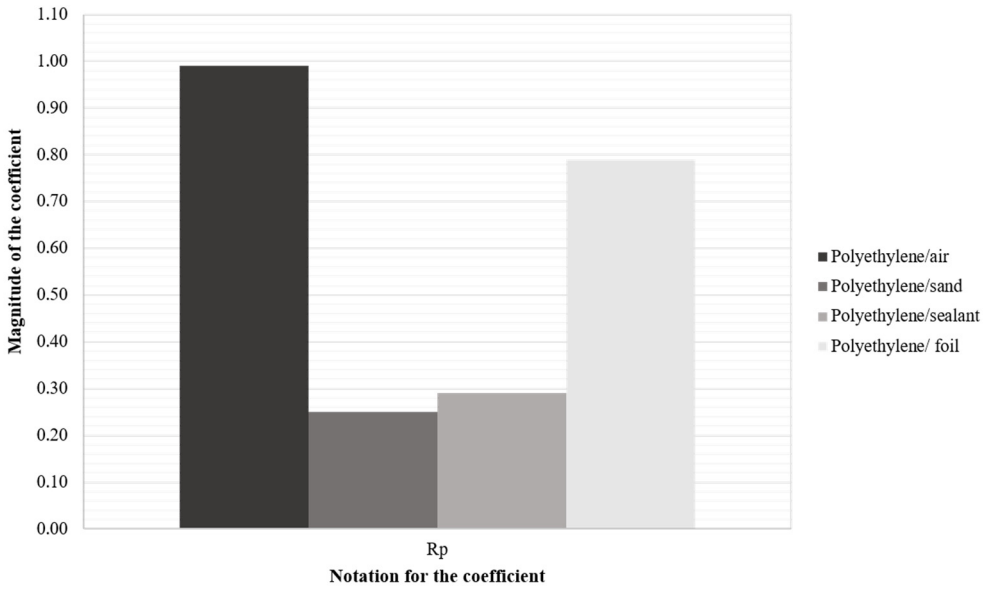


Figure 3. Reflection coefficient values at polyethylene interfaces with other media.

As evident from the obtained results, the reflection coefficients at Type 2 and 3 interfaces are nearly identical, indicating the potential use of this material for manufacturing reference reflectors in calibration specimens.

It should also be noted that if an inhomogeneity detected in the test object represents a gas pore or lack of fusion (Type 1 interface), this discontinuity will still be classified as a defect when the rejection sensitivity level is calibrated using the sealant-based reflector.

To confirm the theoretical analysis results, laboratory studies were conducted using digital radiography and manual ultrasonic testing with chord-type transducers.

2.3. Sound Field Modeling

To verify the applicability of the specular reflection assumption for ultrasonic waves interacting with discontinuities in the test object, wave propagation modeling in polyethylene was performed using COMSOL Multiphysics v. 6.2 software. The developed 2D axisymmetric model includes four key components: an ultrasonic vibration source represented by a linear segment positioned at 45° along the prism boundary, a prism, a 10 mm thick polyethylene plate as the test object, and a 4 mm^2 discontinuity (Figure 4a). The transducer was modeled with a center frequency of 1.8 MHz. Wave propagation was

simulated using the Elastic Waves, Time Explicit physics interface. Boundary conditions were specified as follows: normal vibration velocity was applied at the source, absorbing layers were implemented at the test object's external boundaries to eliminate wave reverberation artifacts, and free boundary conditions were assigned to both the top and bottom surfaces of the polyethylene plate.

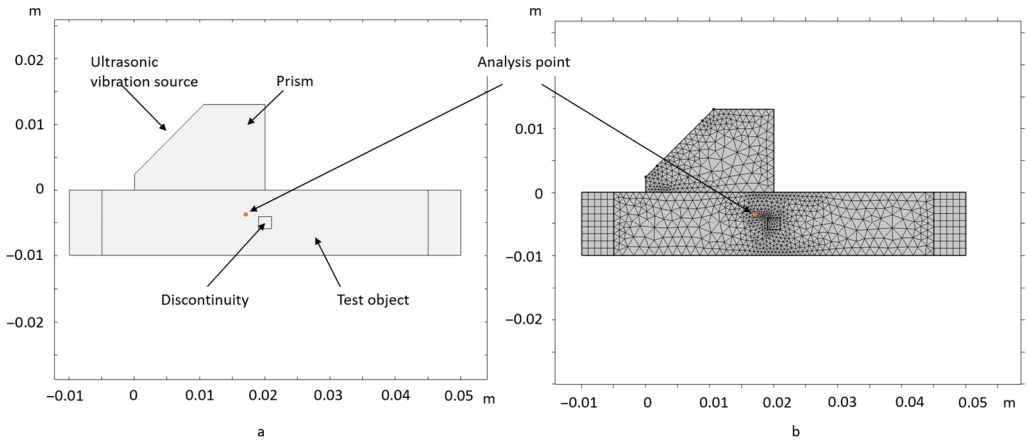


Figure 4. Model visualization: (**a**) geometry configuration; (**b**) finite element mesh.

The model utilizes triangular mesh elements with local refinement near the source, where the minimum element size was selected based on the wavelength. For the absorbing layers, a "mapped" type mesh was implemented (Figure 4b). A solution time of 200 µs was chosen, which allows sufficient time for the ultrasonic wave to completely reflect from the discontinuity.

The simulation yielded the acoustic pressure magnitude at the analysis point for both the incident wave and the wave reflected once from the discontinuity. Figure 5 shows the acoustic pressure distribution for (a) the incident wave and (b) the reflected wave, specifically for a foil inclusion discontinuity.

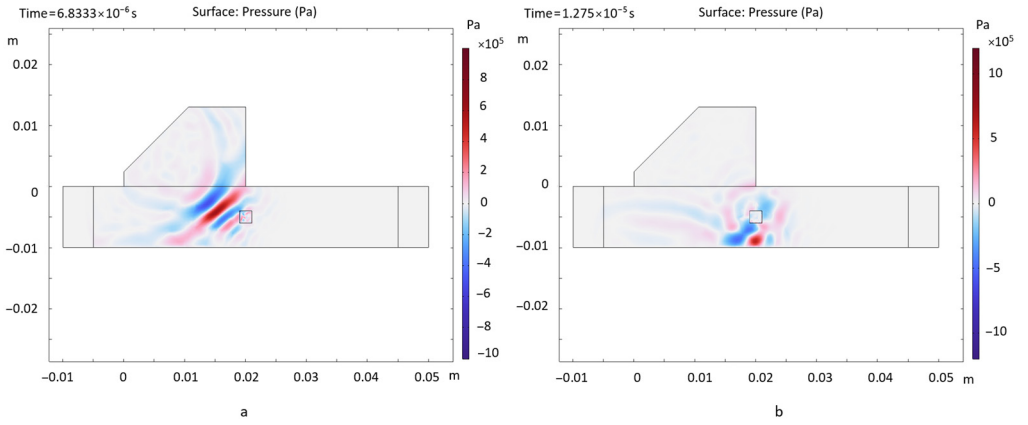


Figure 5. Acoustic pressure distribution: (**a**) incident wave; (**b**) reflected wave.

The simulation produced, for each discontinuity type, a pressure–time waveform plot near the discontinuity (Figure 6). The acoustic pressure values at the points marked in Figure 6 were used to calculate the reflection coefficient (Equation (1)). The specific points selected for pressure measurement were determined based on the time-of-arrival characteristics of the waves at the analysis point.

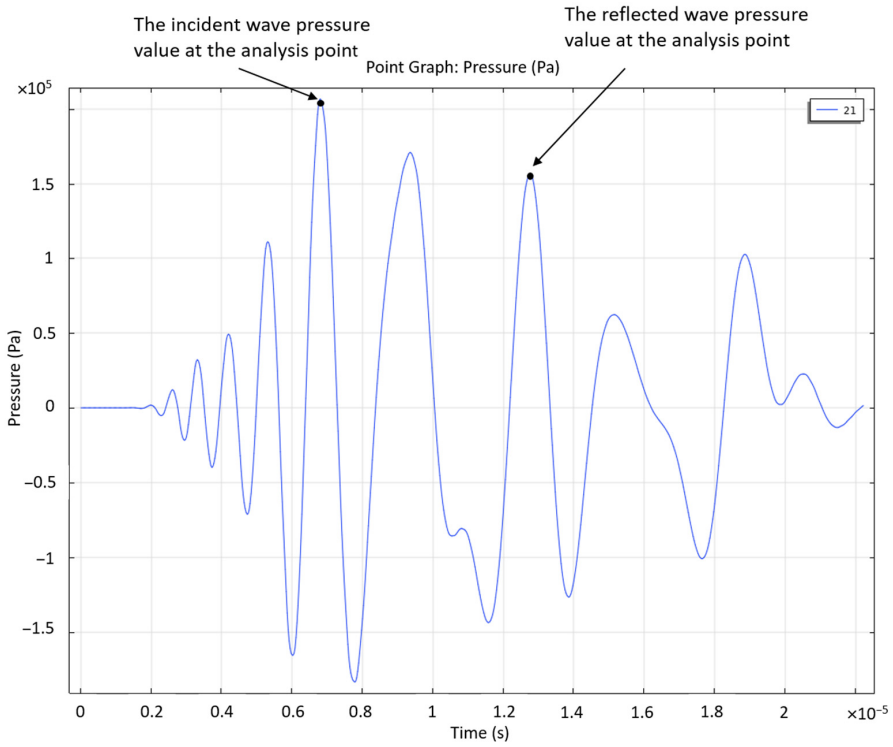


Figure 6. Ultrasonic wave pressure variation.

The modeling yielded simulated reflection coefficients for discontinuities with different fill materials (Table 3). Unlike the reflection coefficients shown in Table 2, the simulated results demonstrate reduced values. This reduction is attributed to the inclusion of the directivity-field-to-reflector-area ratio factor in the modeling.

Table 3. Model reflection coefficients at the boundary of polyethylene and other media.

No. (Type)	Material	Interface Type	$\lvert R_p \rvert$ (Model)
1	Air	Polyethylene/air	0.86
2	Sand	Polyethylene/sand	0.22
3	Heat-resistant silicate sealant	Polyethylene/sealant	0.26
4	Aluminum foil	Polyethylene/foil	0.76

2.4. Sample Preparation

Test specimens were fabricated from PE100 SDR11 polyethylene pipes (outer diameter: 110 mm; see Figure 7). The dimensions of artificial discontinuities are listed in Table 4.

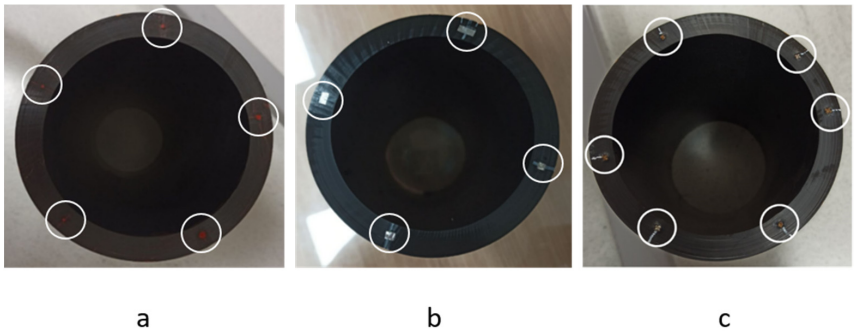


Figure 7. External view of discontinuities in the form of (**a**) sealant; (**b**) foil; (**c**) sand.

Table 4. Geometric dimensions of defects.

No.	Inhomogeneity Material	Cross-Sectional Area, mm^2	Linear Dimensions, mm
1	Aluminum foil	4.0	2.0 × 2.0
2		8.0	4.0 × 2.0
3		12.0	6.0 × 2.0
4		16.0	8.0 × 2.0
5	Heat-resistant silicate sealant	0.9	Ø1.1
6		1.3	Ø1.3
7		1.7	Ø1.5
8		3.1	Ø2.0
9		7.1	Ø3.0
10	Sand	2.5	Ø1.8
11			
12		3.1	Ø2.0
13			
14		3.8	Ø2.2
15			

The simulation of discontinuities using sealant and sand was performed by filling flat-bottom cylindrical holes of corresponding diameter at the pipe end, while foil-type discontinuities were adhered to the pipe's end surface immediately prior to welding.

To determine the acoustic parameters of the heat-resistant sealant, a 100 × 100 mm cube was fabricated, after which its density and longitudinal wave velocity were measured using the PULSAR-2.2 [52] ultrasonic instrument via the through-transmission method [29,53].

Welding was performed using a ZHCN-160E semi-automatic butt-welding machine [54]. Key welding parameters are listed in Table 5.

Table 5. Primary welding parameters for investigated specimens.

No.	Parameter Name	Value
1	Heater temperature	220 °C
2	Bead-up pressure	15 bar
3	Heating time	99 s
4	Cooling time	10 min

2.5. Localization of Inhomogeneities

Following welding, the inhomogeneities within the weld seam were localized using digital radiography performed on the TRANSKAN [55] automated digital radiography system for the X-ray inspection of circumferential pipe welded joints.

2.6. Ultrasonic Testing

Ultrasonic testing was conducted for the following purposes:

1. Analysis of the reflectivity of embedded discontinuities: The relationship between the amplitude of the reflected signal and the geometric dimensions of the discontinuities was determined.
2. Evaluation of defect detectability when calibrating the rejection sensitivity level using different reflector types: Sensitivity levels (in this study, the calibrated sensitivity level was designated as the rejection threshold) were established for reflectors of identical dimensions but with varying filler materials. Subsequently, ultrasonic testing was performed on specimens containing a known quantity of artificially introduced discontinuities in the form of sand inclusions with uniform dimensions.

The ultrasonic testing was performed using a universal ultrasonic flaw detector USD-50 IPS [56] and a chord-type transducer with an ultrasonic frequency of 1.8 MHz. The ultrasonic testing parameters are presented in Table 6.

Table 6. Key ultrasonic testing parameters.

No.	Parameter Name	Value
1	Transducer Type	Chord-type
2	Beam Entry Angle	90° "along the chord"
3	Operating Frequency	1.8 MHz
4	Wave Propagation Velocity	2150 m/s
5	Wavelength	1.3×10^{-3} m
6	Piezoelectric Element Size	Ø1.8 mm
7	Scanning Zone Width	35 mm

The schematic diagram of ultrasonic testing for the polyethylene pipe welded joint using a chordal piezoelectric transducer is shown in Figure 8. Figure 9 demonstrates an example of inspecting a butt-welded joint containing sealant inclusion discontinuities.

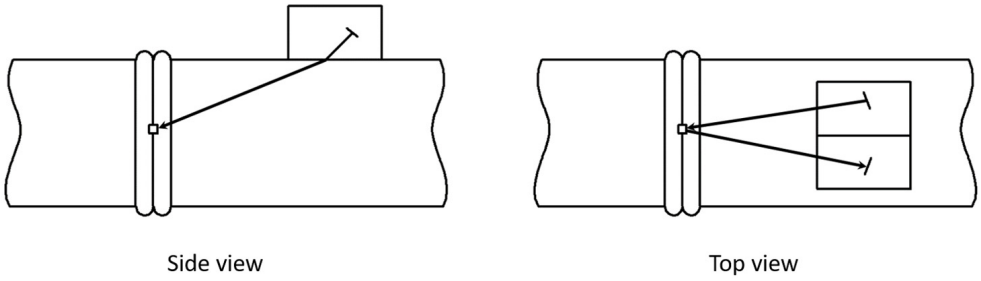


Figure 8. Schematic diagram of ultrasonic testing using a chord-type transducer.

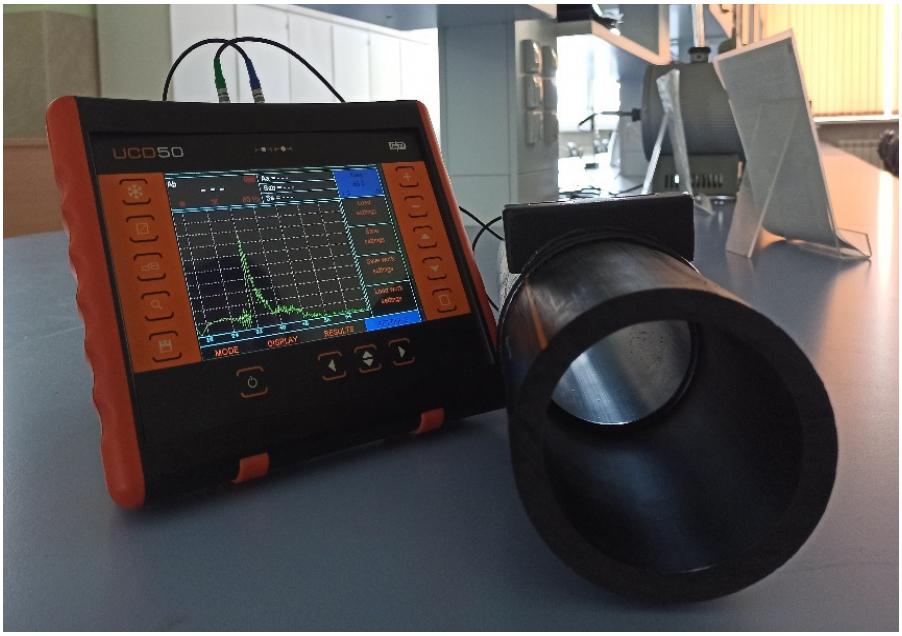


Figure 9. Example of butt weld inspection using a chord-type transducer.

3. Results

3.1. Radiographic Testing

Radiographic images of the welded joint containing foil inclusions are presented in Figure 10, while Figure 11 shows the joint with sealant inclusions.

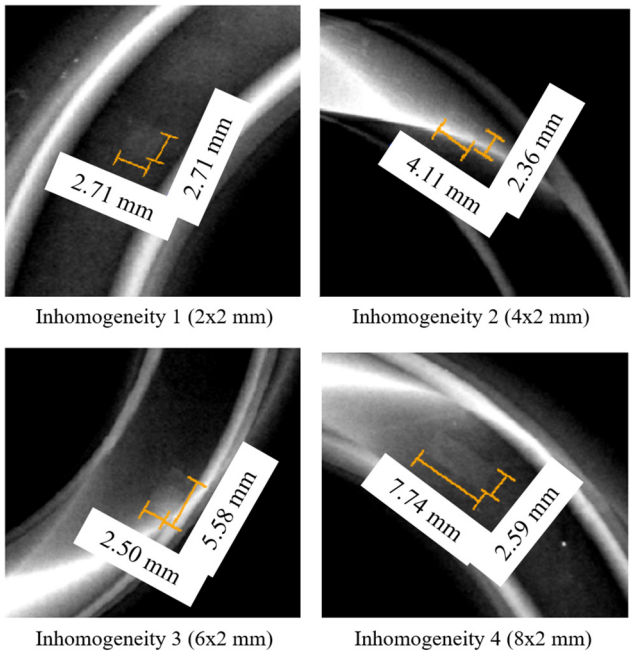


Figure 10. Inhomogeneities in the form of foil inclusions detected by digital radiography.

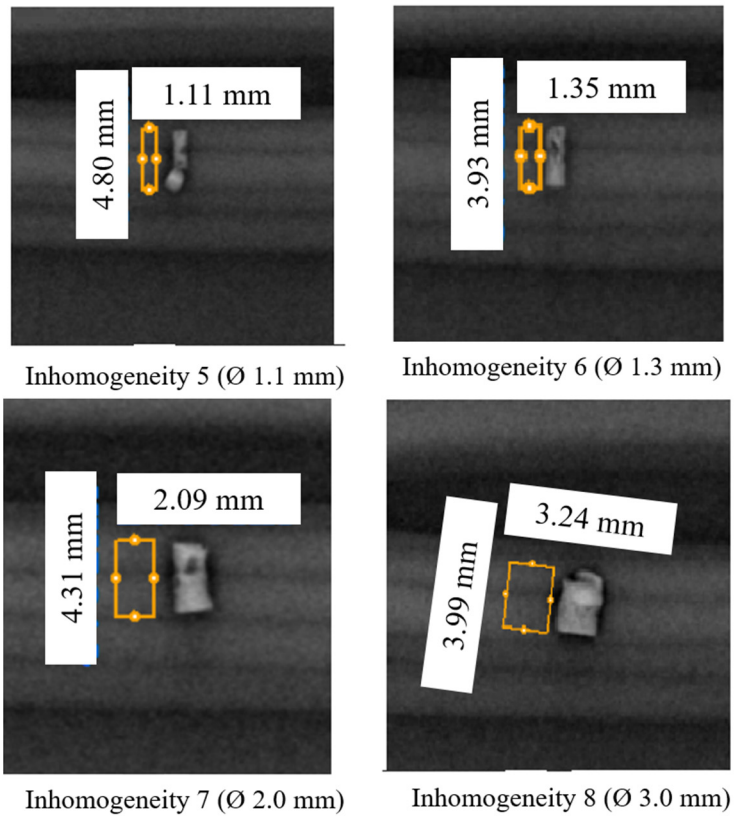


Figure 11. Inhomogeneities in the form of sealant inclusions detected by digital radiography.

Radiographic testing revealed that foil inclusions may shift from their original positions during the welding process (Inhomogeneity 3, Figure 10), while sealant inclusions maintain their geometric position relative to the pipe wall centerline. Moreover, the geometric dimensions of inclusions with different fill materials undergo varying degrees of change during welding. The actual post-weld dimensions of foil inclusions deviated from their original specifications by an average of 25%, compared to just 13% for sealant inclusions.

Based on these measured geometric parameters, it can be concluded that simulating discontinuities using sealant is preferable to foil-based simulation methods.

3.2. Ultrasonic Testing Results

Figures 12 and 13 display the signal amplitudes obtained from foil and sealant inclusions, respectively. As evident from the data, the reflected signal amplitudes from sealant inclusions demonstrate a monotonic decrease with reducing cross-sectional area of the discontinuity, unlike the foil inclusions. The reflected signal amplitude from Inhomogeneity 3 (Figure 12) is significantly lower compared to others in this series. This phenomenon can be attributed to the displacement of this particular discontinuity from the pipe wall centerline during welding, resulting in signal detection only by the upper portion of the transducer's acoustic field (radiation pattern). This observation substantiates the conclusion about the preferential use of sealant for discontinuity simulation.

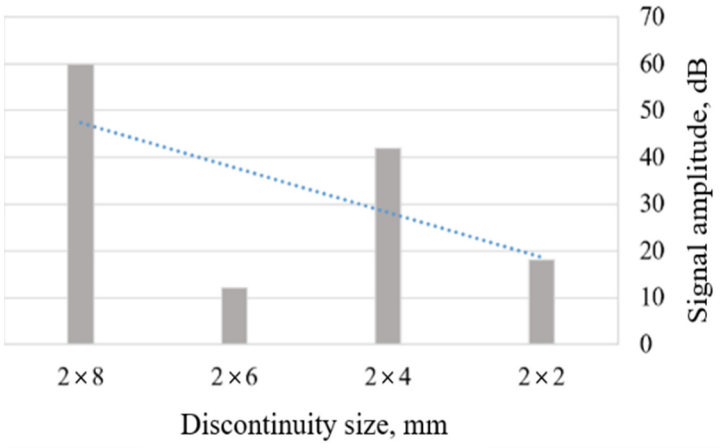


Figure 12. Amplitude of signal reflected from foil inclusion-type discontinuities.

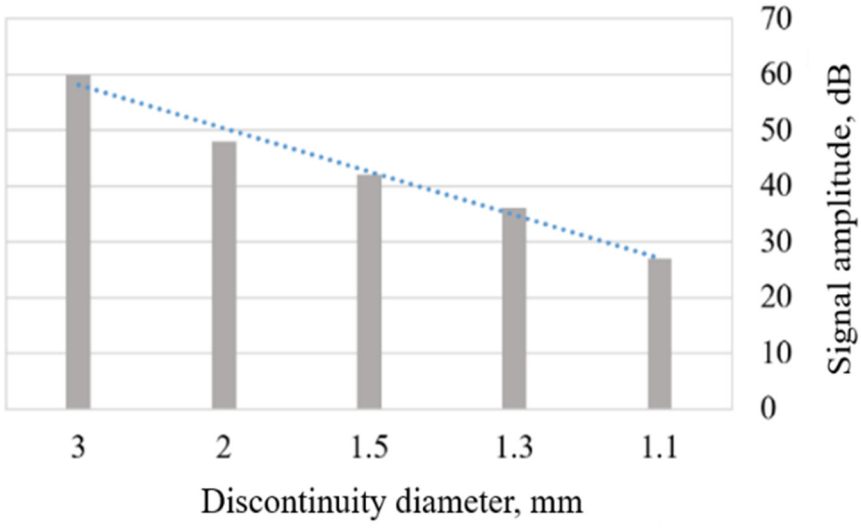


Figure 13. Amplitude of signal reflected from sealant inclusion-type discontinuities.

Subsequently, the amplitudes of signals reflected from sand inclusions were analyzed relative to two distinct rejection sensitivity levels: one calibrated using a flat-bottom hole reflector and another calibrated using sealant inclusions (Figure 14).

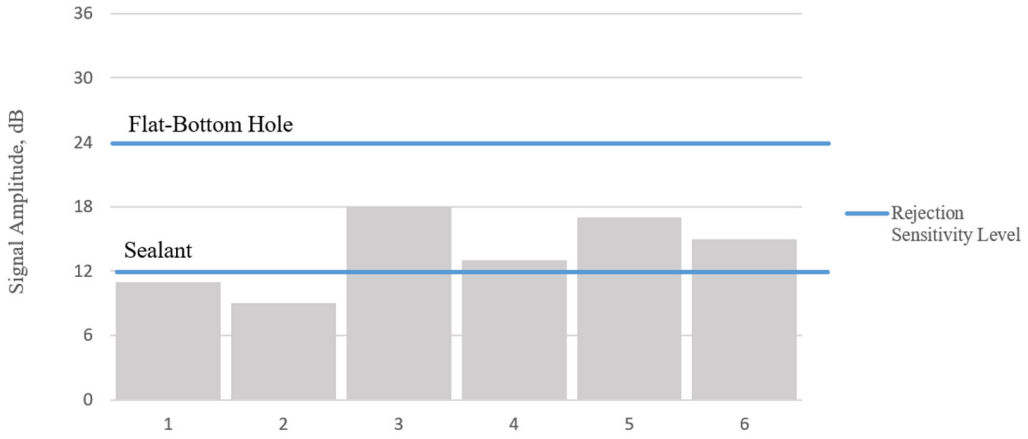


Figure 14. Amplitudes of signals reflected from sand inclusions of identical sizer.

As evidenced by the data, the amplitude of signals reflected from sand inclusions exceeds the rejection sensitivity level calibrated using sealant-type discontinuities, while remaining significantly below the rejection level established using flat-bottom hole reflectors. This results in the erroneous non-classification of sand inclusions as defects—constituting a Type I error (under-rejection).

When calibrated with flat-bottom hole reference reflectors, none of the sand inclusions were classified as defects. In contrast, calibration using sealant-type discontinuities correctly identified four out of six sand inclusions as rejectable defects.

4. Conclusions

The obtained results show that inhomogeneities in the form of sealant inclusions can be used as artificial reflectors in calibration specimens. However, further metrological certification of such specimens is required, including determining the standard deviation and coefficient of variation of geometric and acoustic parameters of this type of artificial reflector during manufacturing.

Additionally, it is necessary to establish the equivalent reflector size that is maximally permissible for a given pipe size. This parameter can be determined through axial tensile and long-term tensile testing.

1. Unlike the acoustic field parameters of signals reflected at the polyethylene/air interface, the acoustic field parameters of signals reflected at the polyethylene/sealant interface are equivalent to those from real defects in welded joints of polyethylene pipelines. At the same time, the reflectivity of air inclusions remains the highest, which enables the detection of all defect types when the rejection sensitivity level is calibrated using sealant-type inhomogeneities.
2. When manufacturing sealant-type inhomogeneities, their geometric and physical-mechanical parameters undergo only minor changes, allowing for a preliminary conclusion on the feasibility of confirming metrological characteristics during specimen certification.
3. The use of calibration specimens with sealant-type inhomogeneities in pulse-echo testing enables the classification of both gas inclusions and solid inclusions as defects, thereby covering all defect types. This approach enhances the reliability of ultrasonic testing for welded joints in polyethylene pipelines.

Author Contributions: Conceptualization, K.G.; methodology, A.S.; formal analysis, K.G.; investigation, D.K. and A.S.; data curation, D.K. and A.V.; writing—original draft preparation, D.K., A.S., and A.V.; writing—review and editing, K.G. and A.Z.; visualization, D.K. and A.V.; supervision, K.G. and A.Z. All authors have read and agreed to the published version of the manuscript.

Funding: This research received no external funding.

Institutional Review Board Statement: Not applicable.

Informed Consent Statement: Not applicable.

Data Availability Statement: The original contributions presented in this study are included in the article. Further inquiries can be directed to the corresponding author.

Conflicts of Interest: Author Aleksei Zubarev was employed by the company A3 Engineering. The remaining authors declare that the research was conducted in the absence of any commercial or financial relationships that could be construed as a potential conflict of interest.

References

1. Nasiri, S.; Khosravani, M.R. Failure and fracture in polyethylene pipes: Overview, prediction methods, and challenges. *Eng. Fail. Anal.* **2023**, *152*, 107496. [CrossRef]
2. Bolobov, V.I.; Zhuikov, I.V.; Popov, G.V. The influence of pipe stress state on the pitting corrosion rate of oilfield pipelines. *Pet. Eng.* **2023**, *21*, 109–120. [CrossRef]
3. Kim, J.-S.; Oh, Y.-J.; Choi, S.-W.; Jang, C. Investigation on the thermal butt fusion performance of the buried high density polyethylene piping in nuclear power plant. *Nucl. Eng. Technol.* **2019**, *51*, 1142–1153. [CrossRef]
4. Wang, Q.; Zhou, H.; Xie, J.; Xu, X. Nonlinear ultrasonic evaluation of high-density polyethylene natural gas pipe thermal butt fusion joint aging behavior. *Int. J. Press. Vessel. Pip.* **2021**, *189*, 104272. [CrossRef]
5. Majid, F.; Elghorba, M. HDPE pipes failure analysis and damage modeling. *Eng. Fail. Anal.* **2017**, *71*, 157–165. [CrossRef]
6. Lebedev, A.; Cherepovitsyn, A.E. Waste Management during the Production Drilling Stage in the Oil and Gas Sector: A Feasibility Study. *Resources* **2024**, *13*, 26. [CrossRef]
7. Rivas, E.Y.; Vyacheslavov, A.; Gogolinskiy, K.V.; Sapozhnikova, K.; Taymanov, R. Deformation monitoring systems for hydroturbine head-cover fastening bolts in hydroelectric power plants. *Sensors* **2025**, *25*, 2548. [CrossRef]
8. Pryakhin, E.I.; Azarov, V.A. Comparative analysis of the use of epoxy and fluoroplastic polymer compositions as internal smooth coatings of the inner cavity of steel main gas pipelines. *CIS Iron Steel Rev.* **2024**, *28*, 93–98. [CrossRef]
9. Kuzmin, K.A.; Sultanbekov, R.R.; Khromova, S.M.; Vovk, M.A.; Rudko, V.A. Establishing the influence of recycled used oil on the sedimentation stability of residual marine fuel. *Fuel* **2025**, *389*, 134625. [CrossRef]
10. Popov, G.V.; Bolobov, V.I.; Zhuikov, I.V.; Zlotin, V.V. Development of the kinetic equation of the groove corrosion process for predicting the residual life of oil-field pipelines. *Energies* **2023**, *16*, 7067. [CrossRef]
11. Grigorev, E.G.; Nosov, V.V. Improving quality control methods to test strengthening technologies: A multilevel model of acoustic pulse flow. *Appl. Sci.* **2022**, *12*, 4549. [CrossRef]
12. Cherepovitsyn, A.E.; Lebedev, A. Drill Cuttings Disposal Efficiency in Offshore Oil Drilling. *J. Mar. Sci. Eng.* **2023**, *11*, 317. [CrossRef]
13. Gazprom Group Social Responsibility Report 2023 [Electronic Resource]. Available online: https://sustainability.gazpromreport.ru/2023/ (accessed on 12 January 2025).
14. Dai, L.S.; Wang, D.P.; Wang, T.; Feng, Q.S.; Yang, X.Q. Analysis and comparison of long distance pipeline failures. *J. Pet. Eng.* **2017**, *2017*, 3174636. [CrossRef]
15. Pshenin, V.V.; Dzhemilev, E.N.; Rozanova, L.I.; Komarovskiy, M.A. The results of the analysis of accident rates of gas distribution systems. *Probl. Gather. Treat. Transp. Oil Prod.* **2022**, *4*, 89–101. [CrossRef]
16. Shi, J.; Feng, Y.; Tao, Y.; Guo, W.; Yao, R.; Zheng, J. Evaluation of the seismic performance of butt-fusion joint in large diameter polyethylene pipelines by full-scale shaking table test. *Nucl. Eng. Technol.* **2023**, *55*, 3342–3351. [CrossRef]
17. Bowman, J. A review of the electrofusion joining process for polyethylene pipe systems. *Polym. Eng. Sci.* **1997**, *37*, 674–691. [CrossRef]
18. Kafieh, R.; Lotfi, T.; Amirfattahi, R. Automatic detection of defects on polyethylene pipe welding using thermal infrared imaging. *Infrared Phys. Technol.* **2011**, *54*, 317–325. [CrossRef]
19. Chen, S.; Lai, H.S.; Lin, R.; Duan, X.H. Study on the creep properties of butt fusion-welded joints of HDPE pipes using the nanoindentation test. *Weld. World* **2021**, *66*, 135–144. [CrossRef]

20. Kuzmin, K.A.; Ivkin, A.S.; Vovk, M.A.; Rudko, V.A. Pour point depressant efficacy for diesel fuels with different n-paraffin distribution. *Fuel* **2025**, *392*, 134885. [CrossRef]
21. Rao, J.; Zeng, L.; Liu, M.; Fu, H. Ultrasonic defect detection of high-density polyethylene pipe materials using FIR filtering and block-wise singular value decomposition. *Ultrasonics* **2023**, *134*, 107088. [CrossRef]
22. Silva, W.; Lopes, R.; Zscherpel, U.; Meinel, D.; Ewert, U. X-ray imaging techniques for inspection of composite pipelines. *Micron* **2021**, *145*, 103033. [CrossRef] [PubMed]
23. Loseva, E.; Lozovsky, I.; Zhostkov, R. Refining Low Strain Pile Integrity Testing for Minor Flaw Detection with Complex Wavelet Transform. *Civ. Eng. J.* **2024**, *10*, 3194–3207. [CrossRef]
24. Wang, B.; Zhong, S.; Lee, T.-L.; Fancey, K.S.; Mi, J. Non-destructive testing and evaluation of composite materials/structures: A state-of-the-art review. *Adv. Mech. Eng.* **2020**, *12*, 1687814020913761. [CrossRef]
25. Kumpati, R.; Skarka, W.; Ontipuli, S.K. Current trends in integration of nondestructive testing methods for engineered materials testing. *Sensors* **2021**, *21*, 6175. [CrossRef]
26. El-Hawwat, S.; Shah, J.; Wang, H.; Venkiteela, G. Detection of internal cracks in polyethylene pipes using ultrasonic imaging and deep learning. *Measurement* **2025**, *253*, 117491. [CrossRef]
27. Piao, C.; Lee, J.; Kim, S.H.; Kim, Y.Y. Ultrasonic inspection of sludge accumulated in plastic pipes using meta-slab mode-converting wedge transducers. *NDT E Int.* **2023**, *142*, 103020. [CrossRef]
28. Tian, Y.; Palaev, A.G.; Shammazov, I.A.; Ren, Y. Non-destructive testing technology for corrosion wall thickness reduction defects in pipelines based on electromagnetic ultrasound. *Front. Earth Sci.* **2024**, *12*, 1432043. [CrossRef]
29. Said-El Hawwat, S.; Shah, J.K.; Wang, H. Machine learning supported ultrasonic testing for characterization of cracks in polyethylene pipes. *Measurement* **2025**, *240*, 115609. [CrossRef]
30. Piao, C.; Kim, S.H.; Lee, J.K.; Choi, W.G.; Kim, Y.Y. Non-invasive ultrasonic inspection of sludge accumulation in a pipe. *Ultrasonics* **2022**, *119*, 106602. [CrossRef]
31. Pshenin, V.V.; Sleptsov, A.A.; Dukhnevich, L.V. Prospects of improving the vibroacoustic method for locating buried non-metallic pipelines. *Eng* **2025**, *6*, 121. [CrossRef]
32. Zarei, A.; Pilla, S. Laser ultrasonics for nondestructive testing of composite materials and structures: A review. *Ultrasonics* **2024**, *136*, 107163. [CrossRef]
33. *GOST R 56510-2015*; Metrological Support in the Field of Non-Destructive Testing. Standartinform: Moscow, Russia, 2019; p. 6.
34. Mihaljević, M.; Markučič, D.; Runje, B.; Keran, Z. Measurement uncertainty evaluation of ultrasonic wall thickness measurement. *Measurement* **2019**, *137*, 179–188. [CrossRef]
35. Yoshida, T.; Wada, S.; Furuichi, N. A calibration methodology of ultrasonic transducers: Evaluation of spatial propagation characteristics of pulse-echo. *Measurement* **2023**, *214*, 112783. [CrossRef]
36. Van Neer, P.L.M.J.; Matte, G.; Sijl, J.; Borsboom, J.M.G.; de Jong, N. Transfer functions of US transducers for harmonic imaging and bubble responses. *Ultrasonics* **2007**, *46*, 336–340. [CrossRef] [PubMed]
37. Santos, D.S.; Baldini, L.; Vos, H.J.; Verweij, M.D.; de Jong, N.; van Neer, P.L.M.J. Acoustic streaming-based calibration of ultrasound transducers. *Appl. Acoust.* **2024**, *217*, 109863. [CrossRef]
38. Kretov, E.F. *Ultrasonic Flaw Detection in Power Engineering*; Sven Publishing House: St. Petersburg, Russia, 2014; 312p, ISBN 978-5-91161-014-2. (In Russian)
39. Mogilner, L.Y.; Syasko, V.A.; Shikhov, A.I. Modeling Defects in Ultrasonic Nondestructive Testing: State-of-the-Art and Prospects. *Russ. J. Nondestruct. Test.* **2024**, *60*, 481–500. [CrossRef]
40. Kusot 180 [Kusot 180]. Constanta-US. Available online: https://constanta-us.com/catalog/nabor_kusot_180/kusot_180_nabor_3/ (accessed on 1 August 2025).
41. Aleshin, N.P.; Mogilner, L.Y.; Shchipakov, N.A.; Kusyi, A.G.; Tishkin, V.V.; Degtyarev, M.N. On the use of grooves for crack simulation in ultrasonic testing. *Russ. J. Nondestruct. Test.* **2022**, *58*, 3–12.
42. Mogilner, L.Y.; Smorodinsky, Y.G. Ultrasonic testing: Application of cylindrical drilling for equipment calibration and verification. *Russ. J. Nondestruct. Test.* **2018**, *54*, 14–20. [CrossRef]
43. Reference Specimen, Flat With Notch [Nastroechnyy Obrazets, Ploskiy s Zarubkoy]. Constanta-US. Available online: https://www.constanta-us.com/catalog/nastroechnye_obraztsy_no/nastroechnyy_obrazets_no_ploskiy_s_zarubkoy/ (accessed on 1 August 2025).
44. *GOST R 8.637-2007*; State System for Ensuring the Uniformity of Measurements. Certified Reference Materials for Metrological Maintenance of Pipeline Non-Destructive Testing Equipment. General Requirements. Standartinform: Moscow, Russia, 2008; p. 6.
45. *ISO 13588:2012*; Non-Destructive Testing of Welds—Ultrasonic Testing—Use of Automated Phased Array Technology. International Organization for Standardization: Geneva, Switzerland, 2019; p. 24.
46. Xu, X.; Chang, Z.; Dou, R.; Ma, X.; Chen, M.; Wu, H.; Yang, K.; Jin, H. Ultrasonic internal multiple migration: An imaging method for defect characterization in complex-structure welds. *Mech. Syst. Signal Process.* **2025**, *231*, 112640. [CrossRef]

47. Chandler, M.G.; Croxford, A.J.; Wilcox, P.D. Defect detection in the presence of geometrical artefacts. *NDT E Int.* **2024**, *142*, 103014. [CrossRef]
48. Wang, H.; Li, Y.; Wang, F.; Zhang, G.; Xie, J.; Zhang, S. Development of an ultrasonic system for nondestructively detecting flaws in the rail foot of in-service railway. *Measurement* **2025**, *251*, 117289. [CrossRef]
49. *GOST R 50.04.07-2022*; Conformity Assessment System for the Nuclear Power Use. Conformity Assessment in the Form of Tests. Qualification Tests of Non-Destructive Inspection Systems. Russian Institute for Standardization: Moscow, Russia, 2022; p. 41.
50. Isakovich, M.A. *General Acoustics: Textbook [Obshchaya Akustika: Uchebnoe Posobie]*; Nauka, Chief Editorial Board of Physical and Mathematical Literature: Moscow, Russia, 1973; p. 463.
51. *GOST R 54792-2024*; Imperfections in Thermoplastic Welding Joints. Descriptions and Evaluation. Russian Institute for Standardization: Moscow, Russia, 2022; p. 28.
52. PULSAR-2.2 Ultrasonic Flaw Detector for Construction Materials Testing//Interpribor: Website. Available online: https://www.interpribor.ru/ultrasonic-flaw-detector-the-pulsar-2.2 (accessed on 11 March 2025). (In Russian).
53. Ermolov, I.N.; Vopilkin, A.K.; Badalyan, V.G. *Calculations in Ultrasonic Flaw Detection: A Concise Handbook [Raschety v Ul'trazvukovoy Defektoskopii: Kratkiy Spravochnik]*; Echo + Scientific & Production Center LLC: Moscow, Russia, 2004; p. 108.
54. NOVATECH ZHCN-160E Butt Welding Machine. NOVATECH. Available online: https://nowatech.nt-rt.ru/price/product/103133 (accessed on 24 January 2025). (In Russian).
55. TRANSKAN Digital Radiography System//Digital X-Ray: Website. Available online: https://digital-xray.ru/product/transkan/ (accessed on 24 January 2025). (In Russian).
56. USD-50 IPS Ultrasonic Flaw Detector//Kropus Scientific & Production Center: Website. Available online: https://kropus.com/catalog/ultrazvukovoy-i-akusticheskiy-kontrol/ultrazvukovye-defektoskopy-dlya-kontrolya-svarnykh-soedineniy-i-materiala/ruchnye-defektoskopy/usd-50-ips/ (accessed on 24 January 2025). (In Russian).

Disclaimer/Publisher's Note: The statements, opinions and data contained in all publications are solely those of the individual author(s) and contributor(s) and not of MDPI and/or the editor(s). MDPI and/or the editor(s) disclaim responsibility for any injury to people or property resulting from any ideas, methods, instructions or products referred to in the content.